

CORROSION

The Journal of Science and Engineering

2015 POSTER AWARD RESEARCH LETTERS

Determination of Cathodic and Anodic Charge from Operando X-Ray Tomography Observation of Galvanic Corrosion of Aluminum Alloy 7050-T7451 and 304 Stainless Steel in a Simulated Fastener
Veronica Rafla, Alison Davenport, and John R. Scully

The Influence of Copper Additions and Aging on the Microstructure and Metastable Pitting of Al-Mg-Si Alloys
S.K. Kairy, P.A. Rometsch, C.H.J. Davies, and N. Birbilis

CORROSION SCIENCE

2015 W.R. Whitney Award Lecture: The Effects of Microstructure and Composition on Al Alloy Corrosion
G.S. Frankel

Green Technology: Tannin-Based Corrosion Inhibitor for Protection of Mild Steel
M. Dargahi, A.L.J. Olsson, N. Tufenkji, and R. Gaudreault

On the Role of Zn Pigments Against Natural and Cathodic Overprotection Disbondment of a Multilayer Paint System
M. Echeverría, C.M. Abreu, K. Lau, and C.A. Echeverría

Effect of Surface Condition on Steam Oxidation of Martensitic Steels and Nickel-Based Alloys
J. Zurek and W.J. Quadackers

Statistical Lifetime Modeling of Fe-Ni-Cr Alloys Subject to High-Temperature Corrosion in Waste-to-Energy Production Units
Sheyla Camperos, Jean Michel Brossard, Pascal Floquet, and Daniel Monceau

The Influence of Low Levels of Zinc, Calcium, Gadolinium, Strontium, and Zirconium on the Corrosion of Magnesium for Wrought Applications
X. Xia, J.F. Nie, C.H.J. Davies, W.N. Tang, S.W. Xu, and N. Birbilis

CORROSION ENGINEERING

Underfilm Corrosion of Transmission Tower Cross-Arms Service-Used in a Pacific Coast Area
N. Fuse, A. Naganuma, T. Fukuchi, Y. Hori, M. Mizuno, and K. Fukunaga

Corrosion Behavior of Multi-Phase Stainless Steel in 15% Hydrochloric Acid at a Temperature of 80°C
K. Eguchi, Y. Ishiguro, and H. Ota

Green Technology: Tannin-Based Corrosion Inhibitor for Protection of Mild Steel

M. Dargahi,^{***} A.L.J. Olsson,^{*} N. Tufenkji,^{*} and R. Gaudreault^{†,**}

ABSTRACT

For more than four decades, tannins extracted from renewable resources have been used to protect steam boilers at levels significantly above ASME guidelines. Using tannin-based (green) corrosion inhibitors reduces water and energy consumption, greenhouse gases emissions, and contaminants in effluent wastewaters, while reducing the environmental footprint of industrial processes. The surface adsorptive and corrosion protective properties of a commercial tannin-based corrosion inhibitor (TG 3300) for mild steel were investigated in an alkaline environment using quartz crystal microbalance with dissipation monitoring, open circuit potential, and electrochemical impedance spectroscopy (EIS). The results showed the formation of an effective and stable tannin-based protective layer on mild steel within the first 5 min to 15 min of adsorption. It was found that adsorption of TG 3300 on mild steel can be well described by the Langmuir isotherm. Highly negative values of apparent Gibbs free energy of adsorption ($\Delta G_{ads} = -47.36$ kJ/mol), indicate a spontaneous and strong adsorption of TG 3300 onto the mild steel surface. The results suggest the formation of a TG 3300 protective layer on mild steel, where the highest value of inhibition efficiency was 85% under the applied experimental conditions.

KEY WORDS: corrosion inhibition, green technology, mild steel, surface adsorption kinetics and thermodynamics, tannin molecules

Submitted for publication: May 15, 2015. Revised and accepted: August 11, 2015. Preprint available online: August 11, 2015, <http://dx.doi.org/10.5006/1777>.

[†] Corresponding author. E-mail: rgaudreault@tgwt.com.

^{*} Department of Chemical Engineering, McGill University, Montreal, QC, Canada.

^{**} TGWT Clean Technologies Inc., Longueuil, QC, Canada.

INTRODUCTION

Corrosion and corrosion-induced safety problems are among the main issues in the water industry¹ and because of a global scarcity of water, it is often necessary to recycle process water as much as possible. This, in turn increases the number of cycles in steam boilers, thereby increasing the concentration of corrosive salts inducing higher corrosion rates and other process problems.² To minimize corrosion and corrosion-induced risks and maximize equipment life expectancy, it is crucial to understand the nature and mechanisms by which corrosion occurs and then inhibit it as much as possible.

One of the most common techniques to minimize corrosion in the water industry is the application of corrosion inhibitors, which form a protective (blocking) layer on the metal surface and minimize the access of corrosive electrolytes to the surface.³ Unfortunately, conventional corrosion inhibitors (e.g., phosphates and sulfites) are neither renewable nor have a reliable performance in highly conductive environments. Therefore, developing new, highly protective, and environmentally friendly corrosion inhibitors for steam boilers, hot-water closed-loop systems, pipelines, and tanks is critical.

Tannin-based corrosion inhibitors are becoming popular in the water industry because of their renewable/green nature and their ability to perform under much higher conductive/corrosive environments (8,000 $\mu\text{S}/\text{cm}$ to 10,000 $\mu\text{S}/\text{cm}$) than the ASME guidelines (< 3,000 $\mu\text{S}/\text{cm}$).⁴

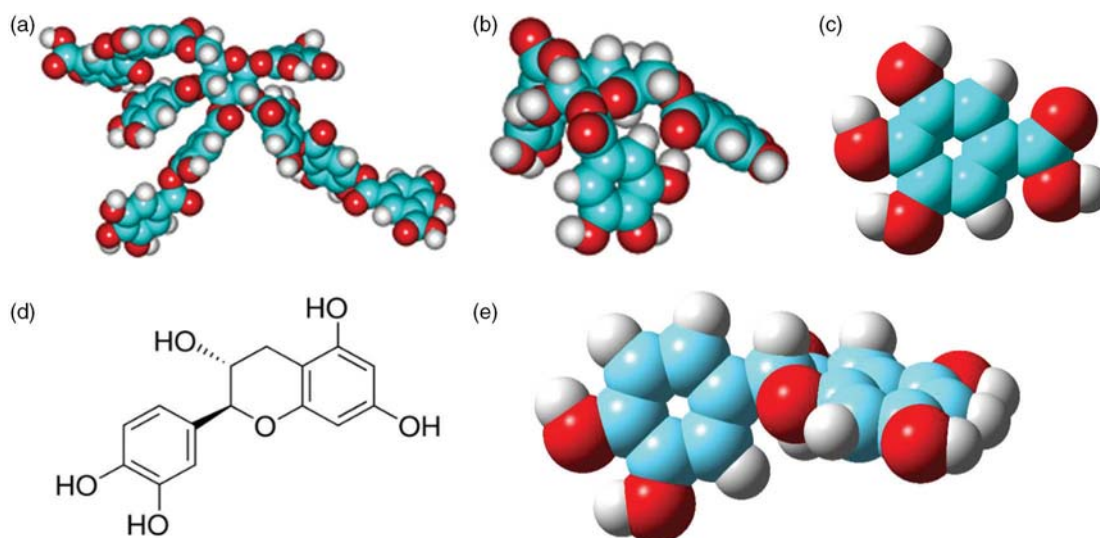


FIGURE 1. Molecular structures of hydrolysable tannins: (a) top view of one possible structure of TA, and (b) TGG; (c) GA,^{6,13} and (d) and (e) condensed tannins, e.g., catechin (courtesy of Professor M.A. [Tony] Whitehead and K. Conley, McGill University).

Although the physicochemical properties of tannin molecules have been studied previously,⁵⁻⁹ the corrosion inhibition properties of these molecules are still poorly understood. In addition, studies on corrosion protective properties of tannin-based corrosion inhibitors have been mostly performed in highly acidic conditions (pH 0.5 to 4.0),¹⁰⁻¹² but rarely in alkaline conditions, which prevail in chilling and heating closed-loop systems.

This work investigated the adsorptive and protective behavior of the tannin-based TG 3300 inhibitor for the protection of mild steel (MS) in alkaline conditions.

MATERIALS AND METHODS

Chemicals and Solutions

The tannin-based TG 3300 inhibitor is a commercial blend of 100% natural molecules such as hydrolysable and condensable tannins (Figure 1, top and bottom respectively^{6,13}), having a charge density of -1.6 equivalent/kg (dry basis) at pH 9.0. The common characteristic of these natural molecules is that they have aromatic rings with hydroxyl and carboxylic groups, and are negatively charged in alkaline pH. Hydrolysable tannins refer to the hydrolysis propensity in highly acidic or alkaline conditions. For example, the hydrolysis of tannic acid (TA), could yield by-products such as 1-3-6-tri-O-galloyl- β -D-glucose (TGG), as well as the ultimate sub-unit, i.e., gallic acid (GA) (Figures 1[a] through [c]). On the other hand, condensed tannins are the most abundant polyphenols, found in virtually all families of plants and comprising up to 50% of the dry

weight of leaves. Tannins of tropical woods tend to be of a cathetic nature, e.g., catechin (Figures 1[d] and [e]), rather than of the gallic-type present in temperate woods.¹⁴ Theoretical molecular modeling methods have been described in previous work.^{6,13}

The tannin-based TG 3300 inhibitor stock solution was prepared by diluting 1 part of concentrated inhibitor with 1 part of deionized water (DI, 18.2 M Ω -cm resistivity), and then further diluting to the desired concentration in DI water to be used as the corrosive solution. For pH adjustment, aqueous 0.1 M sodium hydroxide and 0.1 M sulfuric acid were used. The pH of 10.5 was used for quartz crystal microbalance with dissipation (QCM-D) monitoring, open circuit potential (OCP), and electrochemical impedance spectroscopy (EIS) measurements, while pH 8 to 11 was used for the pH-dependent study.

Quartz Crystal Microbalance with Dissipation Monitoring

An E4 QCM-D[†] unit from Q-Sense was used for the adsorption experiments. MS (C1020, UNS G10200)⁽¹⁾ coated AT-cut quartz custom-made crystals (QSX999) were used as the model substrate. The crystals were cleaned by soaking and sonicating for a minimum of 10 min in a 2% Hellmanex[†] solution (cleaning solution) before being thoroughly rinsed with DI water and dried with nitrogen gas. Then, to remove the organic compounds/contaminations, crystals were exposed to a UV/ozone treatment for 20 min before each experiment. The temperature was controlled by the QCM-D at 22°C and the flow rate of 50 μ L/min was maintained using a peristaltic pump (RegloDigital[†], Ismatec). Before beginning the experiments, a frequency and dissipation baseline in DI water was al-

⁽¹⁾ UNS numbers are listed in *Metals and Alloys in the Unified Numbering System*, published by the Society of Automotive Engineers (SAE International) and cosponsored by ASTM International.

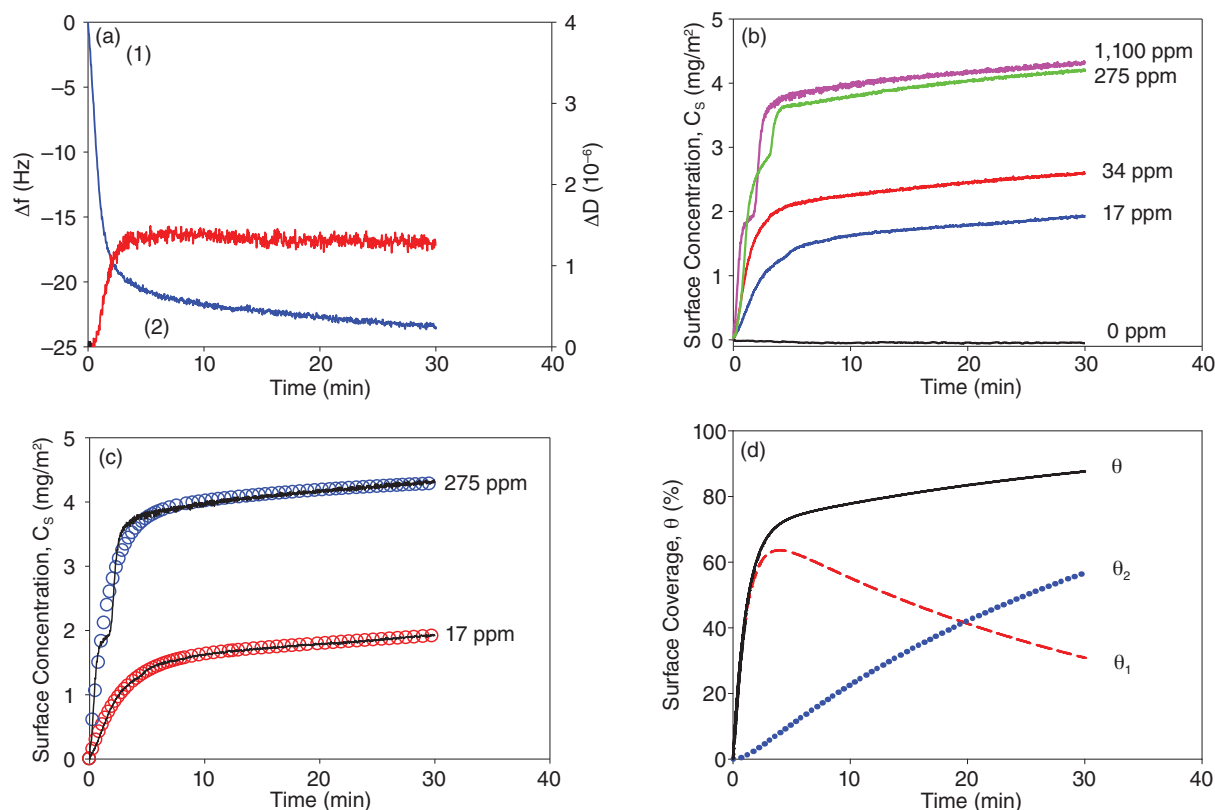


FIGURE 2. (a) Time dependence of adsorbed layer normalized frequency shift and dissipation factor upon adsorption of tannin-based TG 3300 inhibitor obtained from QCM-D in a solution containing 68 ppm of the inhibitor at pH 10.5 and room temperature. (b) Inhibitor surface concentration as a function of time and inhibitor bulk concentration, obtained from QCM-D at pH 10.5 and room temperature. (c) The kinetics of inhibitor adsorption onto the MS surface modeled by the two-step model. Solid lines represent the experimental data, while the circles show simulated data using the kinetic model described by Equations (1) through (3). (d) Time dependence of total relative surface coverage of inhibitor (θ , solid line), relative surface coverage with native (θ_1 , dashed line), and reconformed (θ_2 , dotted line) adsorbed on MS obtained in a solution containing 68 ppm of the inhibitor.

lowed to stabilize. Then, the solution with the desired inhibitor bulk concentration was flowed across the crystal surface. As molecular deposition occurs on the crystal surface, a negative shift in the resonance frequency (Δf) can be measured in real time. After each experiment, the QCM-D setup was cleaned by flowing the cleaning solution and then DI water through the QCM-D for at least 10 min each. The water was purged from the setup using air and nitrogen gas.

To determine whether the Sauerbrey equation provides an adequate estimation of the adsorbed mass, the ratio of the dissipation factor and the normalized frequency shift (normalized with respect to overtone number) was obtained. The threshold value for the Sauerbrey to be valid is 10^{-7} according to the supplier and 4×10^{-7} according to Reviakine, et al.¹⁵ In the present study, the ratio $\Delta D/\Delta f$ was always lower than 10^{-7} (-7.6×10^{-8} to -5.1×10^{-9} Hz⁻¹) for all of the studied inhibitor bulk concentrations, indicating that the protective layer was rigid (Figure 2[a]), and justifying the use of the Sauerbrey equation to calculate the adsorbed mass. Moreover, the frequency shifts were

practically identical at all overtones and therefore only the data from the third overtone is presented.

Consequently, the mass of adsorbed molecules on the QCM-D sensor surface was calculated from the Δf using the Sauerbrey equation, referred to as the Sauerbrey mass.¹⁵

Electrochemical/Corrosion Cell and Equipment

A standard three-electrode electrochemical/corrosion cell was used in the electrochemical experiments. The counter electrode (CE) was a graphite rod. The reference electrode (RE) was a saturated calomel electrode (SCE) separated from the cell by a glass frit. All potentials in this article are expressed with respect to the SCE. The working electrode (WE) was prepared from a C1010 (mild steel, UNS G10100) rod (Metal Samples Company[†]), and sealed with epoxy resin to yield a two-dimensional surface exposed to the electrolyte. Table 1 shows the chemical composition of the alloy used in this study.

Electrochemical measurements were performed using a Solartron 1287[†] electrochemical interface

TABLE 1
The Chemical Composition (% w/w) of Mild Steel

Name	Grade	C	Fe	Mn	P	S
MS C1010	Lab (for electrochemistry experiments)	0.02-0.08	Bulk	0.30-0.60	0-0.04	0.05
MS C1020	Lab (for QCM-D experiments)	0.18-0.23	Bulk	0.30-0.60	0.04	0.05

TABLE 2
Kinetic Rate Constants for the Adsorption of Tannin-Based TG 3300 Inhibitor onto Mild Steel as a Function of Inhibitor Bulk Concentration^(A)

[TG 3300]/ppm	$k_a \times 10^{-5}/M^{-1} \text{ min}^{-1}$	$k_d \times 10/\text{min}^{-1}$	$k_r \times 10^2/\text{min}^{-1}$
17	2.30	2.31±0.08	1.71±0.08
34	2.76	3.36±0.22	1.71±0.31
64	2.94	2.41±0.14	4.07±0.24
275	0.59	0.82±0.23	5.52±0.37
412	0.53	1.64±0.22	3.75±0.18
825	0.21	1.79±0.28	3.83±0.15
1,100	0.12	0.91±0.19	2.32±0.19
1,375	0.11	1.28±0.11	2.41±0.12

^(A) The parameters were determined by fitting the experimental data from QCM-D experiments.

potentiostat/galvanostat and 1260 impedance/gain-phase analyzer. To ensure complete characterization of the interface and the surface processes, EIS measurements were made over a frequency range of 100 kHz to 10 mHz, with an alternating current voltage amplitude of ±10 mV.

Prior to each experiment, the WE surface was polished with 600-gradation abrasive sandpaper, and then thoroughly rinsed with ethanol. After this, the electrode was kept in an ultrasonic bath for 5 min in ethanol, and then rinsed with DI water. The electrode was then immersed in the test electrolyte and equilibrated for 3 h at 70°C at OCP, followed by the electrochemical measurements. All of the solutions were mixed using a magnetic stirrer. All data reported in this work represent mean values of four to six replicates.

RESULTS AND DISCUSSION

Kinetics of Tannin-Based TG 3300 Inhibitor Adsorption on Mild Steel Surface

The kinetics of corrosion inhibitor adsorption was studied to find the time scale within which the MS surface could be covered by varying levels of the inhibitor. Figure 2(b) shows that at a constant inhibitor bulk concentration, the surface concentration of adsorbed inhibitor increased rapidly, and then gradually leveled off to a quasi-steady state. The adsorption equilibrium was reached after ~5 min to 15 min, depending on the inhibitor bulk concentration.

The kinetic data in Figure 2(b) were modeled using a two-step mode.¹⁶⁻¹⁷ For this purpose, the inhibitor surface concentrations were converted into the

corresponding relative surface coverage values ($\theta = (C_{s,t}/C_{s,max})$), where $C_{s,t}$ is the inhibitor surface concentration at time t , and $C_{s,max}$ (~4.25 mg/m²) is the maximum inhibitor surface concentration obtained from the adsorption isotherm (see next section). In the two-step model, the first adsorption step is reversible, and the inhibitor's surface conformation is assumed to resemble that in the bulk solution, i.e., the native conformation. However, the inhibitor with this surface conformation can either desorb (Step 1) or adopt a more thermodynamically favorable surface conformation (Step 2),¹⁶⁻¹⁸ which was assumed to be irreversible.

Expressing the inhibitor surface concentration in terms of its relative surface coverage, θ , the two-step adsorption kinetic model can be formulated as:

$$\frac{d\theta_1}{dt} = k_a[C_i](1 - \theta_1 - \theta_2) - (k_d + k_r)\theta_1 \quad (1)$$

$$\frac{d\theta_2}{dt} = k_r\theta_1 \quad (2)$$

$$\frac{d\theta}{dt} = \frac{d\theta_1}{dt} + \frac{d\theta_2}{dt} = k_a[C_i](1 - \theta) - k_d\theta_1 \quad (3)$$

where $\theta = \theta_1 + \theta_2$ and $0 \leq \theta \leq 1$ are the fraction of relative surface covered by inhibitor in both the thermodynamically unstable (θ_1) and stable (θ_2) conformations, C_i (mol/L) is the inhibitor bulk concentration, k_a ($M^{-1} \text{ min}^{-1}$) is the adsorption constant, k_d (min^{-1}) is the desorption constant, and k_r (min^{-1}) is the reconformation (surface rearrangement) constant.

The experimental data (Figure 2[b]) were fitted using the kinetic model in Equations (1) through (3), and a good agreement between the model (Figure 2[c], circles) and the experimental data (Figure 2[c], solid lines) was obtained in all cases. This shows the applicability of the proposed model to describe the kinetics of inhibitor adsorption onto MS under these experimental conditions (Table 2).

Table 2 shows that for all inhibitor bulk concentrations, the adsorption rate constants were considerably larger than the desorption and reconformation rate constants, showing a strong affinity of inhibitor for MS. In addition, the adsorption kinetic rate constant decreased with an increase in the inhibitor bulk concentration. At higher inhibitor bulk concentrations, the substrate surface became covered by inhibitor faster, which increased the probability for the occurrence of intermolecular interactions. The

decrease in the adsorption rate constants suggests that the intermolecular interactions with the already adsorbed inhibitor molecules inhibit (molecular steric hindrance) further adsorption from the solution.

Molecular reformation kinetics of the inhibitor were also examined. For that purpose, the modeled kinetic data were deconvoluted into the two contributions (θ_1 and θ_2), as shown in Figure 2(d) and then separately in Figures 3(a) and (b). Figures 2(d) and 3(a) demonstrate that the initial increase (within the first 5 min to 10 min of adsorption) in total inhibitor surface coverage, θ (solid line in Figure 2[d]), is mostly a result of the formation of an inhibitor layer with assumed native conformation, θ_1 (dashed line in Figure 2[d]). The surface coverage with the native inhibitor initially increased sharply and then reached a quasi-steady state, which occurred at earlier times at higher bulk solution concentrations. On the other hand, the surface coverage with a reformed inhibitor (Figures 2[d] and 3[b]), θ_2 (dotted line in Figure 2[d]), gradually increased in the entire time interval. Figures 2(d) and 3 also show that the transfer from the native conformation (θ_1) into the reformed inhibitor (θ_2) was not completed within the time interval studied.

In addition, Figure 3(c) shows the values of the ratio of surface coverage of native to reformed adsorbed inhibitor (θ_2/θ_1). The results demonstrated that with an increase in adsorption time, the relative surface ratio also increases. The trend can be approximated by a second-order polynomial function. Also, the values at a particular adsorption time were different at different inhibitor bulk solution concentrations. This indicates that the inhibitor bulk solution concentration influenced the kinetics of the inhibitor surface reformation (from θ_1 to θ_2).

Equilibrium of Tannin-Based TG 3300 Inhibitor Adsorption on Mild Steel Surface

The inhibitor affinity with MS can be determined by the Gibbs free energy of adsorption (ΔG_{ads}), through adsorption isotherms.¹⁸ The mean value of the QCM-D crystal frequency shift, after reaching a quasi-steady state (average of the last 15 min within 1 h of adsorption) at each inhibitor bulk solution concentration, was used for further equilibrium calculations.

Figure 4 shows that the inhibitor surface concentration increased with an increase in inhibitor bulk concentration, and then leveled off to a quasi-steady state (maximum surface concentration, $C_{\text{s,max}} \approx 4.25 \text{ mg/m}^2$) at an inhibitor bulk concentration of approximately 275 ppm. Moreover, the steep initial slope of the adsorption isotherm (rising part of the isotherm) showed the high affinity of TG 3300 molecules for the MS surface.¹⁹

The plot in Figure 4 resembles the shape of a unimodal adsorption isotherm.¹⁸ The corresponding Langmuir isotherm equation, for further investigation of inhibitor adsorption onto MS surface, is:

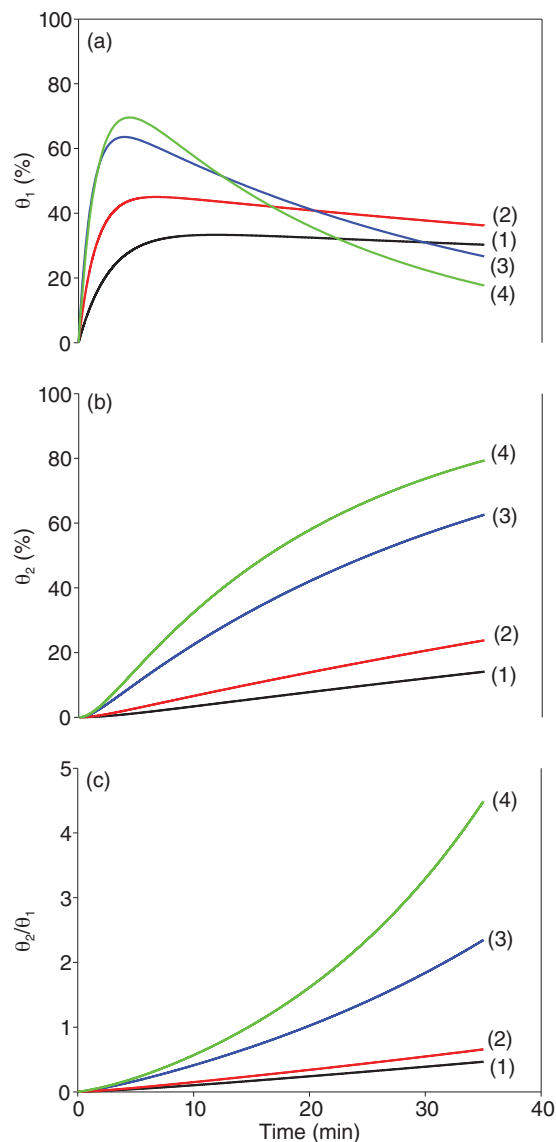


FIGURE 3. Time dependence of MS (a) relative surface coverage with native (θ_1), (b) reformed (θ_2), and (c) the ratio of surface coverage of native to reformed adsorbed inhibitor (θ_2/θ_1) obtained at different tannin-based TG 3300 inhibitor bulk solution concentrations: (1) 17 ppm, (2) 34 ppm, (3) 68 ppm, and (4) 275 ppm.

$$C_{\text{s,i}} = \frac{C_{\text{s,max}} B_{\text{ads}} [C_i]}{1 + B_{\text{ads}} [C_i]} \quad (4)$$

where $C_{\text{s,i}}$ (mg/m^2) is the inhibitor surface concentration at a particular inhibitor bulk concentration, $C_{\text{s,max}}$ ($\sim 4.25 \text{ mg/m}^2$) is the maximum inhibitor surface concentration, B_{ads} (L/mol) is the adsorption affinity constant at constant temperature, and $[C_i]$ (mol/L) is the TG 3300 bulk concentration.

To verify whether the experimental data in Figure 4 can be described by the Langmuir adsorption isotherm, it is more convenient to use a linearized form of Equation (4). Thus, dividing the equation by the

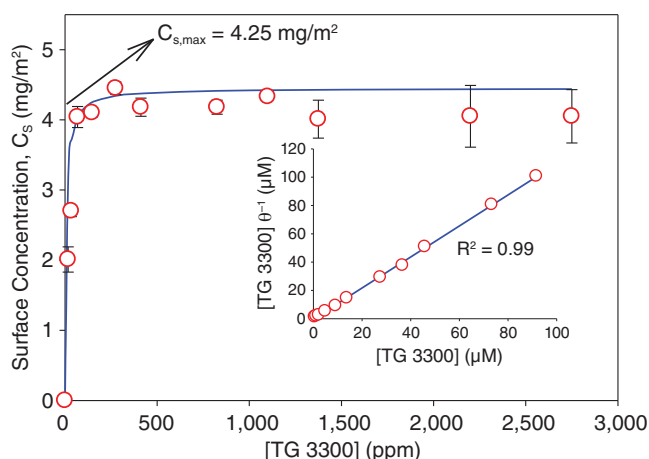


FIGURE 4. Adsorption isotherm for tannin-based TG 3300 inhibitor onto mild steel at pH 10.5 and room temperature. Circles represent the experimental data, while the solid line represents the corresponding value from the Langmuir isotherm. Inset: experimental data (circles) show an excellent correlation with the linearized Langmuir isotherm.

corresponding maximum value ($C_{s,i}/C_{s,max}$) and replacing this ratio with the relative surface coverage, θ_i , a linearized form of the isotherm is obtained:

$$\frac{[C_i]}{\theta_i} = [C_i] + \frac{1}{B_{ads}} \quad (5)$$

For the Langmuir isotherm to be considered valid, a plot of $[C_i]\theta^{-1}$ versus $[C_i]$ should yield a straight line with a slope of 1 and an intercept B_{ads}^{-1} . Indeed, the inset of Figure 4 shows a linear behavior with the corresponding slope close to unity (0.96), in agreement with Equation (5). Consequently, the Langmuir isotherm was deemed applicable in describing the adsorption of inhibitor on MS. From this, the apparent Gibbs free energy of adsorption, ΔG_{ads} (J/mol), was calculated:

$$B_{ads} = \frac{1}{c_{solvent}} \exp\left(\frac{-\Delta G_{ads}}{RT}\right) \quad (6)$$

where $c_{solvent}$ (mol/L) is the molar concentration of the solvent ($c_{water} = 55.5$ mol/L), R is the gas constant (8.314 J/mol·K), and T (K) is the temperature.

The calculated adsorption affinity constant and corresponding apparent Gibbs free energy of adsorption, are $(4.44 \pm 0.21) \times 10^6$ L/mol and -47.36 ± 0.88 kJ/mol, respectively. The relatively large negative apparent Gibbs free energy of adsorption indicated a spontaneous and strong adsorption of inhibitor onto the MS surface.^{18,20}

Other studies¹⁰⁻¹¹ that investigated the adsorption of tannin-based chemistries on MS and aluminum, using gravimetric weight loss at pH 1.0 and 30°C, reported apparent Gibbs free energy of adsorption of

-31.10 kJ/mol and -18.64 kJ/mol, respectively. Although a difference is to be expected as a result of the different surfaces, sensitivity of the techniques, and the overall difficulty of reproducing similar experimental conditions among different research groups, the ΔG_{ads} obtained in the present study were more negative than the literature values, hence indicating a stronger bond between the TG 3300 inhibitor molecules and the MS substrate.

Open Circuit Potential

Figure 5(a) shows the variation of the OCP of MS with time in absence and presence of 137 ppm of tannin-based TG 3300 inhibitor at pH 10.5 and 70°C. In the absence of the inhibitor, the OCP sharply dropped and then reached the quasi-steady state, which indicated MS corrosion in the control solution. However, in the presence of the inhibitor, the OCP value first increased and then reached a plateau. In the first approximation, this trend indicated that the corrosion reaction slowed down with time, and then reached a quasi-steady state rate within the time interval presented here. This indicated blocking of the MS surface by the inhibitor molecules which resulted in less electron transfer between the MS substrate and the bulk solution. Similar results were obtained at other inhibitor bulk concentrations (results not shown here). The mean value of the OCP after reaching a plateau at each inhibitor bulk solution concentration was plotted versus inhibitor bulk concentration (Figure 5[b]). As expected, by increasing the inhibitor bulk concentration, the OCP values approached zero, indicating the adsorption of tannin-based TG 3300 inhibitor on the MS surface and its influence on the corrosion reaction.²¹⁻²²

Electrochemical Impedance Spectroscopy

EIS was applied to investigate the electrode/electrolyte interface and processes that occur on the MS surface at OCP in the presence and absence of the tannin-based TG 3300 inhibitor in solution, most notably the general corrosion resistance of MS. Figure 5(c) shows the EIS spectra of the MS electrode recorded in the absence and presence of the inhibitor at different bulk concentrations. The spectra were recorded at 70°C after the stabilization of the electrode at OCP for 3 h. Figure 5(c) shows that the diameter of the semicircle increased with an increase in inhibitor bulk concentration, indicating an increase in corrosion resistance of the material.²³⁻²⁴

In order to extract quantitative information, a nonlinear least squares fit analysis was used to model the spectra, using electrical equivalent circuits (EECs), presented in Figure 5(d).²⁵⁻²⁶ In these EECs, R_{ci} represents the ohmic resistance between the WE and RE, R_i is the charge transfer resistance related to the corrosion reaction at OCP, and CPE is the capacitance of the electrical double-layer at the electrode/

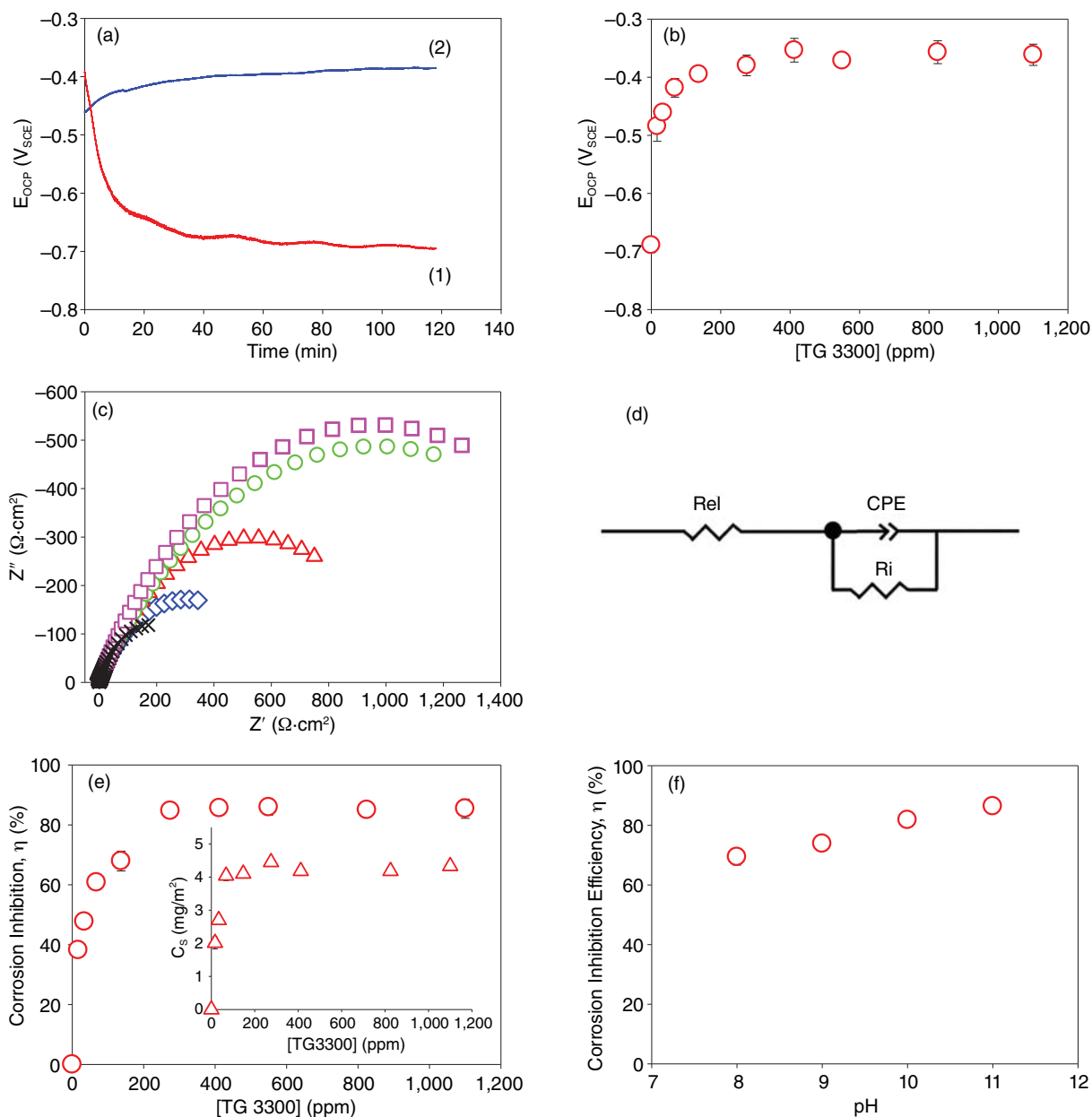


FIGURE 5. (a) OCP of MS as a function of time in the (1) absence and (2) presence (137 ppm) of tannin-based TG 3300 inhibitor at pH 10.5 and 70°C. (b) OCP of MS as a function of inhibitor bulk concentration, recorded after 3 h incubation. (c) Nyquist plot of MS recorded at different bulk concentrations of inhibitor: (x) 0 ppm, (◇) 17 ppm, (△) 68 ppm, (○) 275 ppm, and (□) 550 ppm. (d) EEC model used to fit EIS data recorded for MS in absence and presence of the inhibitor. (e) Corrosion inhibition efficiency of inhibitor as a function of inhibitor bulk concentration. Inset: adsorption isotherm for inhibitor onto mild steel. (f) MS corrosion inhibition efficiency as a function of pH. The EIS data were recorded in the absence and presence of 275 ppm of inhibitor.

electrolyte interface. The EEC in Figure 5(d) was used to fit the spectra recorded in the absence and presence of the inhibitor in the solution and the corresponding EEC values, obtained by fitting the experimental spectra, are presented in Table 3.

The average CPE exponent (0.71 ± 0.02) presented in Table 3 supports the authors' opinion that CPE can be prescribed to the capacitive behavior of the electrochemical double-layer and the adsorbed inhibi-

tor layer. Moreover, the generally decreasing trend of CPE with increasing inhibitor bulk concentration is as expected, and indicates the formation of an adsorbed layer on the MS surface. The increase in the charge transfer resistance R_i also leads to an increase of corrosion inhibition efficiency (η_i).

Taking into account the physical meaning of the EEC parameters of the circuits in Figure 5(d), the corrosion resistance of the bare (control) and covered MS

TABLE 3
Dependence of EEC Parameters on the Concentration of Tannin-Based TG 3300 Inhibitor Bulk Concentration^{(A),(B)}

[TG 3300]/ppm	0	17.1	34.3	68.6	137	275	412	550	825	1,100
CPE $\times 10^6/\Omega^{-1}\cdot\text{cm}^{-2}\cdot\text{s}^n$	586	361	328	274	276	254	271	276	281	252
±SD	35	26	38	43	27	54	19	16	31	42
n_1	0.71	0.73	0.71	0.71	0.69	0.67	0.69	0.69	0.73	0.73
±SD	0.03	0.05	0.03	0.02	0.04	0.05	0.03	0.04	0.03	0.03
Ri/ $\Omega\cdot\text{cm}^2$	419	679	802	1,072	1,315	2,751	2,920	3,048	2,845	2,991
±SD	11	22	26	66	127	258	220	492	436	696
$\eta_i/\%$	0	38.2	47.7	60.8	67.9	84.7	85.6	85.9	85.0	85.4
±SD	0	2.0	1.6	2.5	3.3	1.4	1.1	2.7	2.3	3.2

^(A) The data were obtained by modeling EIS spectra recorded in absence and presence of inhibitor at pH 10.5 and 70°C. The table also lists the corresponding corrosion inhibition efficiency values, η_i .

^(B) SD: standard deviation. An average electrolyte resistance value was 586 Ω .

surface is equivalent to the charge transfer resistance, R_c . Consequently, the corrosion inhibition efficiency (η_i) was calculated by comparing the resistance value, R_c , recorded at various concentrations of inhibitor, and the R_0 value recorded in the absence of inhibitor (control sample; Table 3 and Figure 5[e]):

$$\eta_i = 100 \times \left(1 - \frac{R_0}{R_i} \right) \quad (7)$$

As shown in Figure 5(e), with an increase in the inhibitor bulk concentration, the corrosion inhibition efficiency also increased and reached a maximum value of approximately 85%, indicating high surface corrosion protection. The authors' field data on the protection of MS closed-loop systems, using tannin-based TG 3300 (data not shown), converge with the laboratory results.²⁷ In addition, the calculated trend, in combination with the trend in CPE values (Table 3), indicates that the corrosion inhibition efficiency depends on the inhibitor surface concentration (coverage) that forms the protective layer.

Moreover, the onset of both corrosion inhibition efficiency and the adsorption isotherm occurred at ~275 ppm of inhibitor (Figure 5[e] and the inset). Interestingly, this bulk concentration converges toward the optimum value observed after four decades of empirical optimization in industrial MS boilers and closed-loop systems, treated with tannin-based chemistries.

Effect of pH on Tannin-Based TG 3300 Corrosion Protection of Mild Steel Surface

The influence of pH on MS corrosion inhibition efficiency was studied over a pH range from 8 to 11, in the absence and presence of 275 ppm of tannin-based TG 3300 inhibitor. Figure 5(f) shows that corrosion inhibition increased with pH and gave the highest efficiency at pH 11 (i.e., 86.4±1.60%). This could be a result of the higher corrosion resistance of MS at alkaline pH. The EIS data (not shown here) also confirm higher electron transfer resistance in absence (R_0) and presence (R_i) of inhibitor at alkaline pH. Similar

behavior was observed by the authors in previous work.²⁸

CONCLUSIONS

❖ The QCM-D method was used to investigate the adsorption kinetics and thermodynamics of a tannin-based TG 3300 inhibitor on MS. The kinetic experiments showed that inhibitor adsorption reaches a quasi-steady state within 5 min to 15 min, depending on the inhibitor bulk concentration. The adsorption kinetics follow a two-step model: the first step represents the reversible inhibitor adsorption/desorption, while the second step represents the molecular reformation of tannins into a thermodynamically more stable conformation. The adsorption process showed an excellent correlation ($R^2 = 0.99$) with the Langmuir isotherm. The large negative apparent Gibbs free energy of adsorption ($\Delta G_{\text{ads}} = -47.36$ kJ/mol) confirmed spontaneous and strong adsorption of tannin-based TG 3300 inhibitor on the MS surface. EIS showed that high inhibition efficiency (i.e., 85%) is achieved within 3 h of immersion of a freshly polished MS in the inhibitor solution. Laboratory results showed that by increasing the pH, the MS surface protection increases. Finally, this work is a significant advancement in the field of tannin-based corrosion inhibition of MS because it links the laboratory results with four decades of industrial empirical optimization.

ACKNOWLEDGMENTS

The authors gratefully acknowledge the financial support from the Natural Sciences and Engineering Research Council of Canada (NSERC). The authors also thank Prof. Theo van de Ven from McGill University for valuable scientific insights and Mr. Louis-Philippe Cloutier for valuable discussions.

REFERENCES

1. R. Ebara, F. Tanaka, M. Kawasaki, *Eng. Failure Anal.* 33 (2013): p. 29-36.
2. M. Ash, I. Ash, *Handbook of Corrosion Inhibitor*, 2nd ed. (Houston, TX: NACE International, 2011).

3. M. Fanun, *The Role of Corrosion Inhibitors in Protecting Metallic Structures Against Corrosion in Harsh Environments* (Amsterdam, Netherlands: Elsevier, 2014), p. 509-526.
4. T.J. Tvedt, R.T. Holloway, *Consensus Operating Practices for Control of Feedwater/Boiler Water Chemistry in Modern Industrial Boilers* (New York, NY: ASME, 1994).
5. R. Gaudreault, T.G.M. van de Ven, M.A. Whitehead, *Colloids Surf. A* 268 (2005): p. 131-146.
6. R. Gaudreault, M.A. Whitehead, T.G.M. van de Ven, *J. Phys. Chem. A* 110 (2006): p. 3692-3702.
7. E. Grotewold, *The Science of Flavonoids* (New York, NY: Springer, 2006).
8. J.B. Harborne, H. Baxter, *The Handbook of Natural Flavonoids* (New York, NY: John Wiley and Sons, Inc., 1999).
9. M. Royer, M. Prade, M.E. Garcia-Perez, P.N. Diouf, T. Stevanovic, *PharmaNutrition* 4 (2013): p. 158-167.
10. E.I. Ating, S.A. Umoren, I.I. Udousoro, E.E. Ebenso, A.P. Udoh, *Green Chemistry Letters and Reviews* 3 (2010): p. 61-68.
11. S. Martinez, *Mater. Chem. Phys.* 77 (2003): p. 97-102.
12. L.L. Zhang, Y.M. Lin, H.C. Zhou, S.D. Wei, J.H. Chen, *Molecules* 15 (2010): p. 420-431.
13. R. Gaudreault, "Mechanisms of Flocculation with Poly(ethylene oxide) and Novel Cofactors: Theory and Experiment" (Ph.D. diss., McGill University, 2003).
14. J. Doat, *Bois et Forêts des Tropiques* 182 (1978): p. 34-37.
15. I. Reviakine, D. Johannsmann, R.P. Richter, *Anal. Chem.* 83 (2011): p. 8838-8848.
16. M. Dargahi, S. Omanovic, *Colloids and Surfaces B* 116 (2014): p. 383-388.
17. H. Hennessey, N. Afara, S. Omanovic, A.L. Padjen, *Analytica Chimica Acta* 643 (2009): p. 45-53.
18. M. Dargahi, "Investigation of the Influence of Metal Substrate Surface Charge/Potential on Protein Adsorptive and Biofilm Removal Behaviour" (Ph.D. diss., McGill University, 2014).
19. D. Platikanov, D. Exerowa, *Highlights in Colloid Science* (New York, NY: John Wiley and Sons, Inc., 2008).
20. M. Desroches, S. Omanovic, *Phys. Chem. Chem. Phys.* 10 (2008): p. 2502-2512.
21. U. Rammelt, S. Koehler, G. Reinhard, *Corros. Sci.* 53 (2011): p. 3515-3520.
22. K. Zhang, B. Xu, W. Yung, X. Yin, Y. Chen, *Corros. Sci.* 90 (2015): p. 284-295.
23. S. Ghareba, S. Omanovic, *Corros. Sci.* 52 (2010): p. 2104-2113.
24. S. Ghareba, S. Omanovic, *Electrochim. Acta* 56 (2011): p. 3890-3898.
25. S. Ghareba, S. Omanovic, *Corros. Sci.* 53 (2011): p. 3805-3812.
26. P. Slepski, H. Gerengi, A. Jazdzewska, J. Orlikowski, K. Darowicki, *Construction and Building Materials* 52 (2014): p. 482-487.
27. M. Dargahi, R. Gaudreault, A.J.L. Olsson, N. Tufenkji, "Green Chemistry-Purified Tannin Molecules for the Protection of Mild Steel Closed-Loop Systems," AWT 2014 Annual Convention and Exposition, Fort Worth, TX (Rockville, MD: AWT, 2014).
28. R. Gaudreault, M. Dargahi, N. Weckman, A.J.L. Olsson, S. Omanovic, G. Schwartz, N. Tufenkji, "Green Chemistry—with a Special Emphasis on Tannin Molecules for the Protection of Aluminum Boiler," AWT 2013 Annual Convention and Exposition, Uncasville, CT (Rockville, MD: AWT, 2013).

